Learning and Nonlinear Models - Journal of the Brazilian Society on Artificial Intelligence (SBIA), Vol. 24, Iss. 1, pp. 46–59, 2026
https://doi.org/10.21528/lnlm-vol24-no1-art4 © Brazilian Society on Artificial Intelligence

Modelling, Estimation and Control for an Up-flow Anaerobic Sludge Blanket Reactor Treating Blackwater Towards Resource Recovery

A. Felype F. Maciel, Otacílio B. L. Neto, Michela Mulas
Department of Teleinformatics Engineering, Federal University of Ceará
felypemaciel@alu.ufc.br, otacilio.bneto@proton.me, michela.mulas@ufc.br

Hamse Kjerstadius
Nordvästra Skånes Vatten och Avlopp AB
hamse.kjerstadius@nsva.se

Abstract – This work investigates the model calibration, state estimation, and control of an Up-flow Anaerobic Sludge Blanket (UASB) reactor for the task of increasing its biogas production while complying with effluent quality requirements. We consider a dynamic model based on the Anaerobic Digestion Model No. 1 (ADM1), calibrated using experimental data from a blackwater treatment plant located in Helsingborg, Sweden. Using this model, we design a control solution composed of an operating point optimiser, defining the setpoints that achieve maximum biogas production, and a feedback controller, that tracks these setpoints while rejecting disturbances. For the feedback controller, we consider two alternative approaches: a multiloop Proportional-Integral-Derivate (PID) controller and an output-feedback Model Predictive Controller (MPC). The control solution is showcased on simulated experiments of operating the UASB reactor under different influent disturbance scenarios and compared with the nominal open-loop operation. Our results show that the controlled system is able to increase biogas production, while also improving effluent quality. Both control approaches have similar setpoint tracking performances, with the MPC being more economical and robust to influent disturbances.

Keywords – UASB, System Identification, Feedback Control, State Estimation, Wastewater Treatment, Biogas.

1 Introduction

In a global context where energy demand has steadily increased over recent decades and is expected to continue growing [1–3], Wastewater Treatment Plants (WWTPs) play a crucial role given their significant potential for resource recovery [4]. In this sense, treatment units can rather be seen as Water Resource Recovery Facilities (WRRFs), since water, nutrients, and energy can be obtained from treating wastewater [5]. Anaerobic digestion, for instance, is a biological process widely employed in WWTPs to treat organic matter in the absence of oxygen while simultaneously allowing nutrient recovery and biogas production [6–8]. The methane contained in the biogas can be seen as a green energy source and utilised for heat and electricity generation, thereby supporting the plant's energy demand [9] and reducing the amount of greenhouse gases in the atmosphere [6]. Up-flow Anaerobic Sludge Blanket (UASB) reactors are a particular class of anaerobic digestion systems, characterised by being cost-effective and efficient technologies for organic matter removal, particularly in warm-climate regions [10, 11]. Given the potential for resource recovery, UASB reactors are also used in lower temperatures regions, often integrated with heating systems to improve their operating conditions [12].

Automatic control has been proven to be an essential technology for maximising resource recovery in different types of WWTPs, offering the precision necessary to balance operational efficiency with environmental compliance [13–16]. Proportional-Integral-Derivative (PID) controllers are the most common approach in industry [17, 18]. Conventionally, PID control solutions for WWTPs focused on regulating individual process units based on pre-established targets [19]. More recently, these solutions evolved to incorporate more complex architectures: Revollar et al. [20] proposed a cascade Proportional-Integral (PI) structure to compute the setpoint of dissolved oxygen based on efficiency metrics. Du et al. [21] investigated an event-triggered PID controller for the task of energy-efficient aeration control, while He et al. [22] combined PID control and neural networks for balacing greenhouse gases emissions, operational costs and pollutant discharges through multi-objective optimization. Model Predictive Control (MPC, [23]) is a more advanced method due to its systematic handling of multivariable constraints and the complex coupled dynamics which are commonplace in industrial applications [24]. Because of such advantages, MPC strategies are being widely explored in the context of WWTPs, with focus on energy saving [25], nutrient removal [26–28], disturbance rejection [29–31] or a combination of these objectives [16, 32, 33]. For UASB reactors, feedback control has the potential of enhancing their biogas production, while still ensuring effluents of consistent quality. To the best of the authors' knowledge, [34, 35] are among the few works available studying the optimal control of a UASB reactor. Regrettably, the optimal operation of such processes is yet to be investigated.

Learning and Nonlinear Models - Journal of the Brazilian Society on Artificial Intelligence (SBIA), Vol. 24, Iss. 1, pp. 46–59, 2026
https://doi.org/10.21528/lnlm-vol24-no1-art4 © Brazilian Society on Artificial Intelligence

In this work, we propose a control framework tailored for the optimal operation of UASB reactors. We consider a blackwater treatment facility located in Helsingborg, Sweden, and propose a dynamic model based on the Anaerobic Digestion Model No. 1 (ADM1) [36]. To ensure a realistic representation of the plant's operational dynamics, the model is calibrated through least-squares optimization using historical data. For its operation, we propose a control solution comprised of an Operating Point Optimiser (OPO) and a Feedback Controller (FC). The OPO is responsible for computing a setpoint for maximising biogas production by solving a nonlinear optimization problem with steady-state constraints. The FC tracks these setpoints while rejecting influent disturbances, and we consider two different approaches: a Proportional-Integral-Derivate (PID) controller and an output-feedback Model Predictive Controller (MPC). The controllers are tuned using an approximation of the nonlinear dynamics. The control solution is showcased on simulated experiments of operating the UASB reactor under different influent disturbance scenarios and compared with the nominal open-loop operation. Our results demonstrate that the proposed structure successfully increases the biogas while simultaneously improving the effluent quality.

The paper is structured as follows: Section 2 overviews the UASB reactor, describes its modelling and parameter calibration. Section 3 presents the proposed control solution to operate the UASB reactor for resouce recovery. Section 4 discusses the simulation results on the control of this UASB reactor. Finally, Section 5 provides concluding remarks.

2 The UASB Reactor: Process Layout, Dynamical Model, and Model Calibration

UASB reactors are wastewater treatment systems in which bacteria decompose organic matter in the absence of oxygen, producing treated water, sludge, and biogas in the process [37]. The typical UASB reactor is fed with influent wastewater sludge at its bottom (Figure 1). The lower zone, called the *sludge bed*, is characterised by a high amount of solids, while a lower density of solids happens above the sludge bed, in the *sludge blanket*. Biogas bubbles follow an upward direction as biochemical and physicochemical conversion processes occur in these zones, dragging solids to the upper part of the reactor. A three-phase separator, located at the top of the reactor, ensures that the biogas bubbles and the effluent maintain their respective paths. Heavy sludge particles carried up with the gas bubbles return to the lower zones for further processing. A discharge system is used to remove the excess of sludge and maintain operational efficiency.

This work is based on a reactor located in Helsingborg, Sweden, designed to treat the blackwater generated in one of the city districts, where the collection system separates blackwater, greywater, and food waste [12]. The process layout is illustrated in Figure 1. The collected blackwater is conveyed to the treatment facility and initially stored in a $10\,\mathrm{m}^3$ collection tank. It is then pumped into a $50\,\mathrm{m}^3$ UASB reactor for anaerobic treatment. Excess sludge is periodically withdrawn from the reactor by a manually operated valve and sent to a $2\ \mathrm{m}^3$ sludge tank. The influent flowrate, Q_{in} and the biogas, Q_{gas}, produced in the reactor, are measured by online flowmeters. Excess sludge is removed from the reactor twice a week with a waste flowrate, Q_{w} from $0.8\,\mathrm{m}^3$ to $1.5\,\mathrm{m}^3$ per removal. Influent and effluent quality measurements are obtained from laboratory analyses performed on samples. Besides that, the reactor has sampling points for sludge concentration measurements at every 1 m height intervals. We refer to the original report [12] for the complete details.

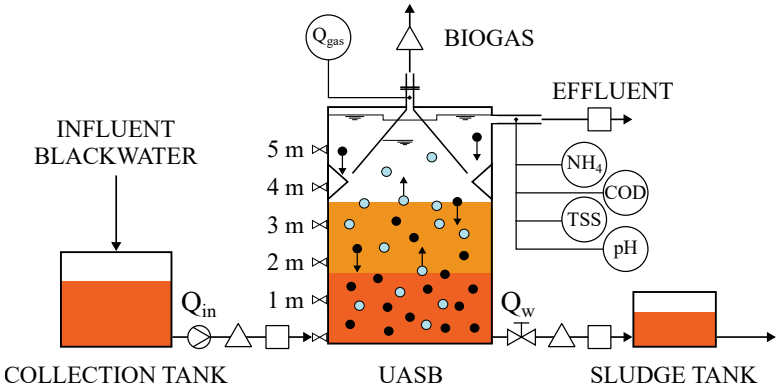


Figure 1: Blackwater treatment system. Blue circles represent biogas bubbles. Black circles are sludge particles. The baloons represent measurable quantities. Adapted from [12, 37].

A 13-week period (26 January 2022 to 20 April 2022) of 1-week averaged data, summarised in Table 1, is considered for this work. The period is selected over a 130-week dataset based on outlier detection, on the absence of missing values, and because it is representative of the system's nominal operation. The data consist of the averaged online flowmeters and the laboratory measurements, whose sampling locations are indicated in Figure 1 by triangles and squares, respectively. During the analysed period, the plant treated on average $41.4\ \mathrm{m}^3$ of blackwater per week. The content of Chemical Oxygen Demand (COD) in the influent ($\mathrm{COD}_{\mathrm{in}}$) was $8.85\,\mathrm{kgCOD/m}^3$ on average. After treatment, the effluent COD ($\mathrm{COD}_{\mathrm{eff}}$), was $1.14\,\mathrm{kgCOD/m}^3$ on average. This corresponds to a 87% COD removal efficiency for the organic compounds, which

https://doi.org/10.21528/lnlm-vol24-no1-art4 © Brazilian Society on Artificial Intelligence

Table 1: Blackwater characteristics.

Variable	Description	Min	Avg	Max	Std	Unit
Q_{in}	Influent flowrate	36.7	41.4	45.9	2.8	m^3/week
Q_{gas}	Biogas flowrate	98.9	111.1	123.2	7.0	m^3/week
COD_{inf}	Influent Chemical Oxygen Demand	7.86	8.85	9.86	0.52	kg/m^3
COD_{eff}	Effluent Chemical Oxygen Demand	0.91	1.14	1.83	0.25	kg/m^3
TSS_{in}	Influent Total Suspended Solids	3.24	4.39	5.10	0.50	kg/m^3
TSS_{eff}	Effluent Total Suspended Solids	0.10	0.20	0.70	0.16	kg/m^3
$NH_{4,in}$	Influent Ammonium	0.97	1.47	2.01	0.34	kg/m^3
$NH_{4,eff}$	Effluent Ammonium	1.08	1.60	2.30	0.45	kg/m^3

is consistent with the observed biogas production of 111.1 m^3 of biogas per week and indicates stable anaerobic digestion performance during the analysed period. The influent total suspended solids (TSS) averaged 4.39 kg/m^3, whereas the effluent presented a substantially lower average concentration of 0.205 kg/m^3. This indicates effective solids retention within the reactor and satisfactory solid-liquid separation performance during operation. As expected, the influent and effluent ammonium concentrations ($NH_{4,in}$ and $NH_{4,eff}$) remained at similar levels during the monitoring period, with average values of 1.47 kgN/m^3 and 1.60 kgN/m^3, respectively, indicating the limited nitrogen removal typically achieved in UASB reactors.

2.1 Dynamical modelling

The dynamic behaviour of UASB reactors can be described using the model by [38]. The model accounts for the density difference in the reactor due to sludge settling by determining different layers with transport of particles transport between them. The reactor is divided into a zone A (Z_A, denoting the *sludge bed*) and a zone B (Z_B, denoting the *sludge blanket*), as depicted in Figure 2. Each zone $Z_{(\cdot)}$ is described by its volume, $V^{(\cdot)}$, and the quantities

$$x^{(\cdot)} = \Big(S_{su}^{(\cdot)},\ S_{aa}^{(\cdot)},\ S_{fa}^{(\cdot)},\ S_{va}^{(\cdot)},\ S_{bu}^{(\cdot)},\ S_{pro}^{(\cdot)},\ S_{ac}^{(\cdot)},\ S_{h2}^{(\cdot)}, S_{ch4}^{(\cdot)},\ S_{ic}^{(\cdot)},\ S_{in}^{(\cdot)},\ S_{i}^{(\cdot)},\ X_{c}^{(\cdot)},\ X_{ch}^{(\cdot)},\ X_{pr}^{(\cdot)},\ X_{li}^{(\cdot)}, X_{su}^{(\cdot)},\ X_{aa}^{(\cdot)},\ X_{fa}^{(\cdot)},\ X_{c4}^{(\cdot)},\ X_{pro}^{(\cdot)},\ X_{ac}^{(\cdot)},\ X_{h2}^{(\cdot)},\ X_{i}^{(\cdot)}, S_{cat+}^{(\cdot)},\ S_{an-}^{(\cdot)},\ S_{va-}^{(\cdot)},\ S_{bu-}^{(\cdot)},\ S_{pro-}^{(\cdot)},\ S_{ac-}^{(\cdot)},\ S_{hco3-}^{(\cdot)},\ S_{nh3}^{(\cdot)}, S_{g,h2}^{(\cdot)},\ S_{g,ch4}^{(\cdot)},\ S_{g,co2}^{(\cdot)}\Big), \quad (1)$$

consisting of the concentrations of different soluble ($S^{(\cdot)}$) and particulate ($X^{(\cdot)}$) components in that zone. The dynamics in each zone are based on the ADM1 [36], as described below. The sludge bed volume V^{A} evolves in time according with

$$\dot{V}^{\mathrm{A}} = \frac{1}{\rho^{\mathrm{A}}}\left(Q_{\mathrm{in}}X_{\mathrm{T,in}} + Q_{\mathrm{dn}}^{\mathrm{B}}X_{\mathrm{T}}^{\mathrm{B}} - (Q_{\mathrm{up}}^{X} + Q_{\mathrm{w}})X_{\mathrm{T}}^{\mathrm{A}} + V^{\mathrm{A}}r_{X_{\mathrm{T}}}^{\mathrm{A}}\right) \quad (2)$$

where ρ^{A} is the sludge density, Q_{in} is the influent flowrate (with $X_{\mathrm{T,in}}$ being the influent total concentration of solids), $Q_{\mathrm{dn}}^{\mathrm{B}}$ is the downwards flowrate of solids from Z_{B} to Z_{A} (with total concentration $X_{\mathrm{T}}^{\mathrm{B}}$), $\{Q_{\mathrm{up}}^{X}, Q_{\mathrm{w}}\}$ are the upwards flowrate of solids from Z_{A} to Z_{B} and the wastage flowrate, respectively (with total concentration $X_{\mathrm{T}}^{\mathrm{A}}$), and $r_{X_T}^{\mathrm{A}}$ is the sum of reaction rates associated with solid matter in Z_{A} as described by [36]. The sludge blanket volume is $V^{\mathrm{B}} = V^{\mathrm{AB}} - V^{\mathrm{A}}$, where V^{AB} is the liquid volume in the reactor, and thus $\dot{V}^{\mathrm{B}} = -\dot{V}^{\mathrm{A}}$. The soluble components, $S^{(\cdot)}$, have dynamics of the form

$$\dot{S}^{(\cdot)} = \frac{1}{V^{(\cdot)}}\Big(Q_{\mathrm{in}}S_{\mathrm{in}}^{(\cdot)} - (Q_{\mathrm{in}} + \dot{V}^{(\cdot)})S^{(\cdot)}\Big) + r_{S}^{(\cdot)} \quad (3)$$

with $S_{\mathrm{in}}^{\mathrm{A}}$ being the influent concentrations of that component, $S_{\mathrm{in}}^{\mathrm{B}} = S^{\mathrm{A}}$, and $r_{S}^{(\cdot)}$ being the reaction rates as described in [36]. In this model, note that the upwards flowrate of soluble matter from Z_{A} to Z_{B} is assumed equal to the influent flowrate Q_{in}. Finally, the particulate components, $X^{(\cdot)}$, evolve as

$$\dot{X}^{\mathrm{A}} = \frac{1}{V^{\mathrm{A}}}\Big(Q_{\mathrm{in}}X_{\mathrm{in}}^{\mathrm{A}} - (Q_{\mathrm{up}}^{X}+Q_{\mathrm{w}}+\dot{V}^{\mathrm{A}})X^{\mathrm{A}} + Q_{\mathrm{dn}}^{\mathrm{B}}X^{\mathrm{B}}\Big) + r_{X}^{\mathrm{A}} \quad (4)$$

$$\dot{X}^{\mathrm{B}} = \frac{1}{V^{\mathrm{B}}}\Big(Q_{\mathrm{up}}^{X}X^{\mathrm{A}} - (Q_{\mathrm{out}}^{X}+Q_{\mathrm{dn}}^{\mathrm{B}}+\dot{V}^{\mathrm{B}})X^{B}\Big) + r_{X}^{\mathrm{B}} \quad (5)$$

where Q_{up}^{X} is the upwards flowrate of solids from Z_{A} to Z_{B}, Q_{out}^{X} is the outflow of particulates leaving the UASB reactor, and $r_{X}^{(\cdot)}$ are the reaction rates described in [36].

Learning and Nonlinear Models - Journal of the Brazilian Society on Artificial Intelligence (SBIA), Vol. 24, Iss. 1, pp. 46–59, 2026
https://doi.org/10.21528/lnlm-vol24-no1-art4 © Brazilian Society on Artificial Intelligence

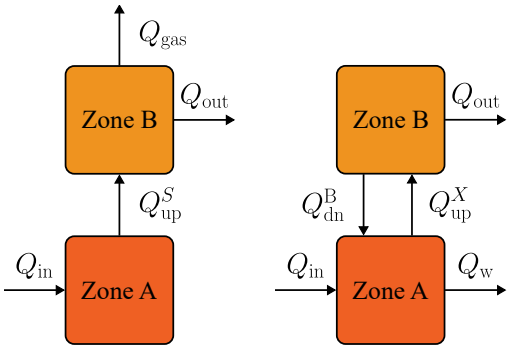


Figure 2: Movement of soluble (left) and particulate (right) components in the UASB model. Adapted from [38].

In this model, we assume a sensor arrangement capable of producing real-time measurements of the quantities

$$y = \big(V^{\text{A}},\ Q_{\text{gas}},\ \text{TSS}_{\text{eff}},\ \text{COD}_{\text{eff}},\ \text{NH}_{4,\text{eff}},\ \text{pH}\big), \tag{6}$$

with Q_{gas} being the flowrate of biogas leaving the reactor, and TSS_{eff}, COD_{eff}, $\text{NH}_{4,\text{eff}}$, and pH, being the effluent total suspended solids, chemical oxygen demand, concentrations of ammonium, and potential of hydrogen, respectively. The system is assumed to be controlled using an actuation arrangement capable of directly manipulating the quantities

$$u = \big(Q_{\text{in}},\ Q_{\text{w}}\big). \tag{7}$$

Finally, the dynamics of the UASB reactor are also affected by the unmeasurable disturbances w consisting of the influent concentrations of the first 26 components defined in Eq. (1).

Summarising, the state-space model of the UASB is

$$\dot{x}(t) = f(x(t), u(t), w(t) \mid \theta); \tag{8a}$$
$$y(t) = g(x(t), u(t), w(t) \mid \theta). \tag{8b}$$

with states $x(t) = (V^{\text{A}}(t),\ x^{\text{A}}(t),\ x^{\text{B}}(t)) \in \mathbb{R}^{N_x}$, inputs $u(t) \in \mathbb{R}^{N_u}$ and $w(t) \in \mathbb{R}^{N_w}$, and outputs (or measurements) $y(t) \in \mathbb{R}^{N_y}$ as defined in Eqs. (1)–(7). The functions $f(\cdot)$ and $g(\cdot)$ describe, respectively, the dynamic evolution of the $N_x = 1 + 35 + 35$ states and how they are emitted as the $N_y = 6$ outputs, given the $N_u = 2$ actionable inputs and the $N_w = 26$ disturbances. The model depends on a set of constant parameters $\theta \in \mathbb{R}^{103}$, to be calibrated to better represent the physical system of interest. Hereafter, we assume no throughput of the inputs and simply write $y = g(x \mid \theta)$.

2.2 Model calibration

In the following, we present the calibration of the model to better represent the UASB reactor located in Helsingborg, Sweden. Based on literature, we select a subset of parameters, denoted $\theta_{\text{id}} \in \mathbb{R}^{46}$, related to the geometry of the reactor and its physicochemical processes, and then we optimise their values to better match the historical data collected from the real system (Table 1). Furthermore, we fine-tune the model calibration by computing the column-wise sum of the Jacobian matrix $\partial f(\cdot)/\partial\theta_{\text{id}}$, selecting those parameters associated with the $N_y = 6$ largest values, and then reoptimise them based on the same historical data. The remaining parameters are set to their nominal values as reported in [36].

The calibrated parameters $\theta^{\star}_{\text{id}}$ are obtained by solving, using the sequential quadratic programming (SQP) algorithm [39], (constrained) nonlinear least-squares problems of the form

$$\underset{\theta_{\text{id}} \in \Theta}{\text{minimize}} \quad \sum_{t \in \mathcal{T}} \|y^{\text{data}}(t) - y^{\text{pred}}(t \mid \theta_{\text{id}})\|^2_W \tag{9}$$

where $\mathcal{T}$ are the time instants of the samples being considered, $\{y^{\text{data}}(t),\ u^{\text{data}}(t)\}$ are the outputs and input data sampled from the real plant at $t \in \mathcal{T}$, and $y^{\text{pred}}(t \mid \theta_{\text{id}})$ are the corresponding outputs as predicted from the dynamical model (Eq. 8), given the parameter values θ_{id}. In practice, the predictions $y^{\text{pred}}(\cdot)$ are formed as

$$y^{\text{pred}}(t \mid \theta_{\text{id}}) = g(x^{\text{pred}})$$
$$x^{\text{pred}}(t \mid \theta_{\text{id}}) = x_0 + \textstyle\int_0^t f\big(x(\tau), u^{\text{data}}(\tau), w^{\text{data}}(\tau) \mid \theta_{\text{id}}\big),$$

where the state predictions, x^{pred}, are computed using a variable-step variable-order integrator [40]. Finally, $W \succeq 0$ (Eq. 9) is a weighting matrix that can be used to normalize the data, and Θ is the set of admissible parameters; specifically,

$$\Theta = \{\theta_{\text{id}} \in \mathbb{R}^{46} \mid x^{\text{pred}}(t \mid \theta_{\text{id}}) \geq 0,\ \ t \in \mathcal{T}\},$$

Learning and Nonlinear Models - Journal of the Brazilian Society on Artificial Intelligence (SBIA), Vol. 24, Iss. 1, pp. 46–59, 2026
https://doi.org/10.21528/lnlm-vol24-no1-art4 © Brazilian Society on Artificial Intelligence

to ensure that the calibrated model is physically plausible.

The main model calibration results are shown in Figure 3. Despite some inaccuracies, the predicted biogas production follows the trends of the data collected. The predictions of COD_{eff} closely match the data during the first 50 days, and still capture the general trend after that period. The calibrated model achieves a RMSE of 1.31 m^3/d with respect to biogas and a RMSE of 0.19 kg/m^3 with respect to COD_{eff}. As this model captures the general behaviour of the system, it provides a suitable platform for control design.

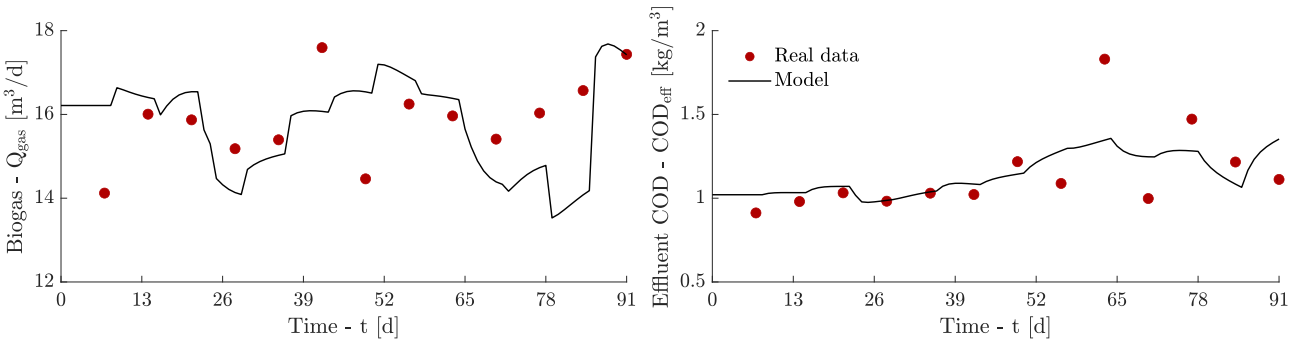


Figure 3: Calibration results for biogas (Q_{gas}), left, and effluent organic matter (COD_{eff}), right.

3 Control architecture: overview and feedback control strategies

In this section, we describe the control architecture designed to operate the UASB reactor (Section 2) for the task of treating blackwater while maximizing biogas production. Our proposal is centered on a feedback control strategy (Figure 4) comprised of two main modules: (i) an operating point optimiser, which determines an equilibrium point (i.e., a steady-state) at which the process achieves the desired operational objective; and a (ii) feedback controller which computes inputs to correct deviations caused by the disturbances and maintain the process around this desired equilibrium. The controller operate in cycles of duration $\Delta t = 0.5$ [days], each starting at time $t_k = k\Delta t$ ($k = 1, 2, \ldots$).

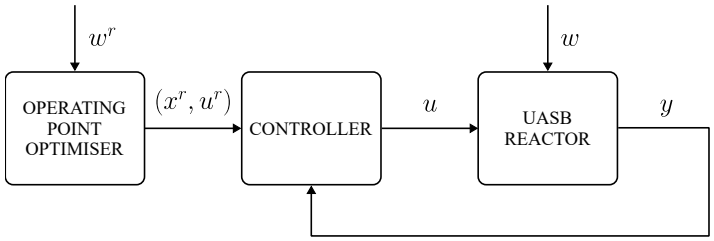


Figure 4: Architecture of the proposed feedback control solution.

3.1 Operating point optimizer (OPO)

At each kth cycle, the OPO determines an operating point that, if enforced, achieves the desired operational objective. In this work, we focus on the task of maximising methane production (MP) while maintaining the effluent COD (COD_{eff}) below some specified quality limit. Formally, this task can be expressed as the (static) optimization problem

$$\underset{x,u}{\text{maximize}} \quad \text{MP} \tag{10a}$$

$$\text{subject to} \quad 0 = f(x, u, w^r \mid \theta), \tag{10b}$$

$$\text{COD}_{\text{eff}} \leq 1, \;\; u \in \mathcal{U}, \tag{10c}$$

where $w^r \in \mathbb{R}^{N_w}$ is the expected influent profile. The quantities $(\text{MP}, \text{COD}_{\text{eff}})$ are computed according to

$$\text{MP} = \frac{16 P_{\text{atm}}}{RT_{\text{op}}} \frac{p_{\text{gas,CH}_4}}{p_{\text{gas,tot}}} Q_{\text{gas}} \tag{11}$$

$$\text{COD}_{\text{eff}} = S^{\text{B}}_{\text{su}} + S^{\text{B}}_{\text{aa}} + S^{\text{B}}_{\text{fa}} + S^{\text{B}}_{\text{va}} + S^{\text{B}}_{\text{bu}} + S^{\text{B}}_{\text{i}} + S^{\text{B}}_{\text{ac}} + X^{\text{B}}_{\text{ch}} + X^{\text{B}}_{\text{pr}} + X^{\text{B}}_{\text{li}} + X^{\text{B}}_{\text{i}}, \tag{12}$$

where P_{atm} is the atmospheric pressure, $p_{\text{gas,CH}_4}$ is the pressure of the methane gas produced, $p_{\text{gas,tot}}$ is the total gas pressure, R is the universal gas law constant, and T_{op} is the operational temperature of the reactor [41].

https://doi.org/10.21528/lnlm-vol24-no1-art4 © Brazilian Society on Artificial Intelligence

A solution to Problem (10) is referred to as an optimal operating point, $r = (x^r, u^r, w^r)$. The equality constraint (Eq. 10b) enforces these optimal operating points to be steady-states (that is, the process can be stabilized around them). The inequality constraints (Eq. 10c) enforce that the operating point satisfy the effluent quality limits ($\text{COD}_{\text{eff}} \leq 1$ kg/m^3) and lies within the actuators' operational limits represented by the set

$$\mathcal{U} = \left\{ \begin{bmatrix} u_1 \\ u_2 \end{bmatrix} \;\middle|\; \begin{bmatrix} 0 \\ 0 \end{bmatrix} \leq \begin{bmatrix} u_1 \\ u_2 \end{bmatrix} \leq \begin{bmatrix} 7.0 \\ 1.4 \end{bmatrix} \right\}. \tag{13}$$

The upper bounds for $u_1 \equiv Q_{\text{in}}$ and $u_2 \equiv Q_{\text{w}}$ are chosen such that the maximum flow corresponds to 70% of the total volumes per day of the collection tank and the sludge tank (Figure 1), respectively.

3.2 Feedback controller (FC)

At each kth cycle, the FC is designed to steer the process towards the optimal operating point $r = (x^r, u^r, w^r)$ by correcting deviations caused by the disturbances. In this work, we design controllers based on linear approximations of the process dynamics around this operating point, which can be expressed as the state space

$$\Delta\dot{x}(t) = A_c\Delta x(t) + B_c\Delta u(t) + G_c\Delta w(t) \tag{14a}$$
$$\Delta y(t) = C\Delta x(t) \tag{14b}$$

with signals in deviation variables (e.g., $\Delta x = x - x^r$). Formally, the controller task is thus to implement a control policy

$$\Delta u(t) = K(\Delta y(t)) \iff u(t) = u^r + K(y(t) - y^r) \tag{15}$$

which drives the state(-deviation) to the origin, $\Delta x \to 0$, thus tracking the optimal reference $x \to x^r$. In this direction, we consider two alternative, well-established options for the control policy: the PID controller and the MPC policies.

Proportional-integral-derivative (PID) controller

A multiple-input-multiple-output PID controller (Figure 5) is based on the policy

$$\Delta u(t) = K_p\Delta y(t) + K_i\int_0^t \Delta y(\tau)d\tau + K_d\tfrac{d}{dt}\Delta y(t) \tag{16}$$

given the user-defined tuning matrices $K_p, K_i, K_d \in \mathbb{R}^{N_u \times N_y}$. In practice, the control policy comprises a proportional, integral, and derivative term, which must be adjusted by the corresponding tuning matrices to achieve a desired response to the output error [18]. The proportional term represents the instantaneous reaction to the error, Δy, being the main component of the control policy. The integral term accounts for the accumulated error until the current time t, thus allowing for correcting any offset between the controlled variable and its reference caused by a constant (or slowly varying) disturbance. The derivative term anticipates the process dynamics, allowing the control policy to improve performance for low-noise systems. Finally, we note that the PID control policy (Eq. 16) does not explicitly enforce actuator limits, so it is common practice to connect a *saturator* to such a controller when designing its parameters.

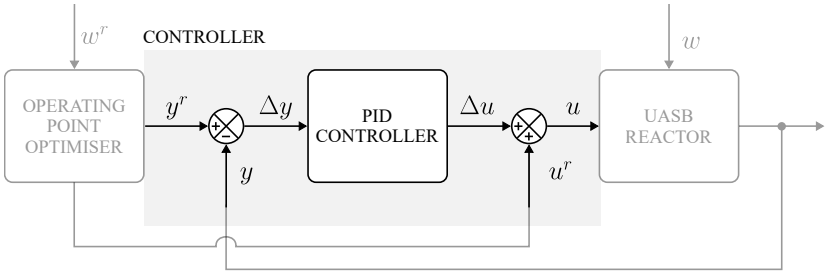


Figure 5: Structure of the PID feedback controller.

In this work, based on process knowledge, we design a simplified PID by directly pairing the inputs ($u_1 \equiv Q_{\text{in}}$ and $u_2 \equiv Q_{\text{w}}$) with the two main outputs we wish to control ($y_2 \equiv Q_{\text{gas}}$ and $y_4 \equiv \text{COD}_{\text{eff}}$), according to the policy

$$\begin{bmatrix} \Delta u_1 \\ \Delta u_2 \end{bmatrix} = \begin{bmatrix} k_{\text{p1}} & \\ & k_{\text{p,22}} \end{bmatrix} \begin{bmatrix} \Delta y_2 \\ \Delta y_4 \end{bmatrix} + \begin{bmatrix} k_{\text{i1}} & \\ & k_{\text{i2}} \end{bmatrix} \begin{bmatrix} \int_0^t \Delta y_2(\tau)d\tau \\ \int_0^t \Delta y_4(\tau)d\tau \end{bmatrix} + \begin{bmatrix} k_{\text{d1}} & \\ & k_{\text{d2}} \end{bmatrix} \begin{bmatrix} d\Delta y_2/dt \\ d\Delta y_4/dt \end{bmatrix}. \tag{17}$$

https://doi.org/10.21528/lnlm-vol24-no1-art4 © Brazilian Society on Artificial Intelligence

In this setup, the control policy corresponds to two independent single-input-single-output (SISO) PIDs. The proportional (k_{p1}, k_{p2}), integral (k_{i1}, k_{i2}), and derivative (k_{d1}, k_{d2}) control parameters are tuned as follows[1]. We first identify linear models of the error responses (based on simulations of the nonlinear model), corresponding to the transfer functions

$$G_1(s) = \frac{\Delta y_2(s)}{\Delta u_1(s)} = \frac{14.44}{(1301s+1)(409s+1)} \quad \text{and} \quad G_2(s) = \frac{\Delta y_4(s)}{\Delta u_2(s)} = \frac{6.98(10.1s+1)}{(0.0945s+1)(8.97s+1)}, \tag{18}$$

obtained from step response data generated by simulating the nonlinear model around $(x_{\text{ref}}, u_{\text{ref}})$ with a perturbation of $0.1\, u_{\text{ref}}$. The transfer functions were chosen to represent second-order responses, since these are sufficient to represent the main dynamics. Then, we form the closed-loop transfer functions for each PID loop (Eq. 17), and modify the tuning parameters until the resulting response is satisfactory [42].

Model predictive controller (MPC)

The MPC (Figure 6) is designed to steer the process towards the optimal operating point (x^r, u^r, w^r) by optimally correcting deviations caused by the disturbances. At each kth cycle, the MPC control policy

$$u(t) = u^r + K_{\text{ocp}}\big(\hat{x}(t_k) - x^r\big), \quad t \in [t_k,\ t_{k+1}), \tag{19}$$

where $K_{\text{ocp}}(\cdot)$ returns the first element of the optimal control(-deviation) sequence $\mathbf{\Delta u}^\star = (\Delta u_0^\star, \ldots, \Delta u_{N-1}^\star)$ solving the finite-horizon optimal control problem

$$\underset{\mathbf{\Delta x}, \mathbf{\Delta u}}{\text{minimize}} \quad \sum_{n=0}^{N-1} \begin{bmatrix}\Delta x_n \\ \Delta u_n\end{bmatrix}^\mathsf{T} \begin{bmatrix} Q & \\ & R\end{bmatrix} \begin{bmatrix}\Delta x_n \\ \Delta u_n\end{bmatrix} + \Delta x_N^\mathsf{T} Q_f \Delta x_N \tag{20a}$$

$$\underset{n=0,\ldots,N-1}{\text{subject to}} \quad \Delta x_{n+1} = A\Delta x_n + B\Delta u_n \tag{20b}$$

$$\Delta x_n \in \Delta\mathcal{X},\ \ \Delta u_n \in \Delta\mathcal{U}, \tag{20c}$$

$$\Delta x_0 = \Delta\hat{x}_k. \tag{20d}$$

The objective function (Eq. 20a) is defined by the tuning matrices $Q \succeq 0$ and $R \succ 0$, which quantify the relative importance of correcting state deviations or input deviations from the operating point, respectively. The final-state weighting matrix, $Q_f \succeq 0$, is particularly important, as its careful tuning can improve closed-loop stability. In this work, we set this matrix as the solution of the discrete-time algebraic Riccati equation (DARE) [18]

$$Q_f = A^\mathsf{T} Q_f A - (A^\mathsf{T} Q_f B)(R + B^\mathsf{T} Q_f B)^{-1}(B^\mathsf{T} Q_f A) + Q.$$

The dynamical constraints (20b) consider a linear dynamical model obtained by *linearizing-then-discretizing* the nonlinear dynamics $f(\cdot)$ around (x^r, u^r, w^r), that is, the matrices (A, B, G) can be obtained from the matrix exponential

$$\begin{bmatrix} A & B & G \\ 0 & I & 0 \\ 0 & 0 & I \end{bmatrix} = \exp\left(\begin{bmatrix} A_c & B_c & G_c \\ 0 & 0 & 0 \\ 0 & 0 & 0 \end{bmatrix} \Delta t\right) \tag{21}$$

with $A_c = (\partial f/\partial x)|_{(x^r,u^r,w^r)}$, $B_c = (\partial f/\partial u)|_{(x^r,u^r,w^r)}$, and $G_c = (\partial f/\partial w)|_{x^r,u^r,w^r}$. The path constraints (Eq. 20c) are defined by the state constraints set $(\Delta\mathcal{X})$ and the input constraints set $(\Delta\mathcal{U})$ describing the feasible deviations around the operating point; in this work, the states are constrained only by the dynamics $(\Delta\mathcal{X} \in \mathbb{R}^{N_x})$, while the input deviations are constrained by the actuator's operational limits $(\Delta\mathcal{U} = \mathcal{U} - u^r$, given Eq. 13). Finally, the boundary condition (Eq. 20d) updates the initial condition of the MPC given a current estimate of the state deviation $(\Delta\hat{x}_k)$.

Under the setup described above, due to Lyapunov's Indirect Method [43], this control policy (locally) stabilizes the UASB reactor around the desired operating point maximizing biogas production; provided that the system does not escape its region of attraction due to the disturbances.

Moving-horizon estimator: The conventional MPC is a state-feedback controller. In order to enable output feedback, we proceed by including a moving-horizon estimator into the control architecture (Figure 6). At each kth cycle, it computes a sequence of optimal state and disturbances deviations $\mathbf{\Delta\hat{x}}^\star = (\Delta\hat{x}_0^\star, \ldots, \Delta\hat{x}_{N_e}^\star)$, $\mathbf{\Delta\hat{w}}^\star = (\Delta\hat{w}_0^\star, \ldots, \Delta\hat{w}_{N_e-1}^\star)$ solving the finite-horizon optimal estimation problem

$$\underset{\mathbf{\Delta\hat{x}}, \mathbf{\Delta\hat{w}}}{\text{minimize}} \quad \Delta e_0^\mathsf{T} Q_0 \Delta e_0 + \sum_{n=1}^{N_e-1} \begin{bmatrix}\Delta e_n \\ \Delta\hat{w}_n\end{bmatrix}^\mathsf{T} \begin{bmatrix} Q_e & \\ & R_e\end{bmatrix} \begin{bmatrix}\Delta e_n \\ \Delta\hat{w}_n\end{bmatrix} + \Delta e_{N_e}^\mathsf{T} Q_e \Delta e_{N_e} \tag{22a}$$

$$\underset{n=0,\ldots,N_e-1}{\text{subject to}} \quad \Delta\hat{x}_{n+1} = A\Delta\hat{x}_n + B\Delta u_n^\star + G\Delta\hat{w}_n \tag{22b}$$

$$\Delta\hat{x}_n \in \Delta\mathcal{X},\ \ \Delta\hat{w}_n \in \Delta\mathcal{W}, \tag{22c}$$

[1]The computations were all performed using the PID Tuner Toolbox from MATLAB©.

https://doi.org/10.21528/lnlm-vol24-no1-art4 © Brazilian Society on Artificial Intelligence

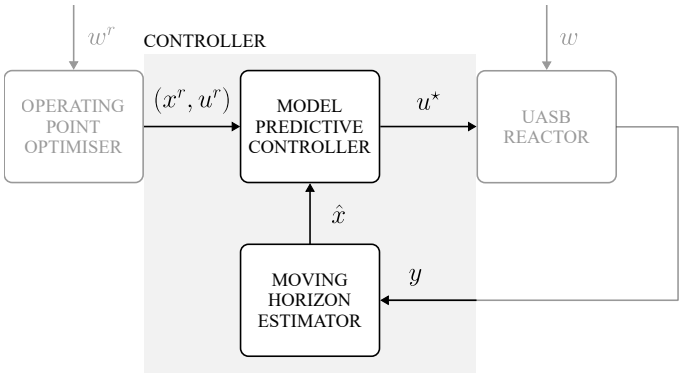


Figure 6: Structure of the MPC feedback controller.

with the auxiliary signal $\Delta e_n = C\hat{x}_n - y_n^{\text{data}}$ denoting the difference between the predicted outputs and the (historic) measurement data, then setting the estimates as $\hat{x}(t_k) = x^r + \Delta\hat{x}^\star_{N_e}$ and $\hat{w}(t_k) = w^r + \Delta\hat{w}^\star_{N_e-1}$. The matrix $Q_e \succeq 0$ quantify the error between the estimated outputs and the measurement data, whereas $R_e \succ 0$ serves as a weighting factor for the difference between the estimated and the reference disturbances. We define both matrices based on the precision matrices of the measurement noise and process disturbance, respectively. The initial weighting matrix Q_0 is particularly important, and chosen to be the solution to the discrete-time algebraic Riccati equation (DARE),

$$Q_0^{-1} = A^\mathsf{T} Q_0^{-1} A - (AQ_0^{-1}C^\mathsf{T})(R_e + CQ_0^{-1}C^\mathsf{T})^{-1}(CQ_0^{-1}A^\mathsf{T}) + Q_e.$$

The disturbances are constrained by a nonnegative lower bound given the reference disturbance values ($\Delta\mathcal{W} = \mathcal{W} - w^r$).

4 Results and Discussion

In this section, we present the simulation results on the estimation and control of the UASB reactor for resource recovery. We consider two scenarios: (i) a nominal scenario, in which the influent conditions are based on the experimental data (Section 2); and an (ii) extreme scenario, in which we simulate episodes of extreme changes in the influent conditions. We consider a period of 3 months ($T = 90$ [days]) and discuss the performance of the controllers against the open-loop operation of the process as outlined in [12]. In both scenarios, a (Gaussian) random process to simulate measurement noise, considering mean and covariance values that represent typical sensor precision. The performance of the controlled system is assessed through its ability to enforce the desired operation (Section 3.1), as well as its operational costs as proportional to the average influent (Q_{in}) and waste (Q_{w}) flow-rates. Additionally, we discuss the average methane production and the effluent quality achieved by the controllers during the evaluation period.

4.1 Operating point optimization

The OPO (Section 3) produces an optimal reference point $r = (x^r, u^r, w^r)$ at which the UASB reactor generates $Q^r_{\text{gas}} = 24.43\,\text{m}^3\text{/d}$ of biogas and $\text{COD}^r_{\text{eff}} = 0.80\,\text{kg/m}^3$ of organic matter. This is achieved when the input references are $Q^r_{\text{in}} = 7\,\text{m}^3\text{/d}$ and $Q^r_{\text{w}} = 1.12\,\text{m}^3\text{/d}$, under the average influent conditions w^r. The optimal reference represents an increase of 60.94% relative to the average biogas production rate of $15.18\,\text{m}^3\text{/d}$ in the nominal open-loop operation shown in Figure 3. In terms of effluent quality, the reference represents a 40.74% reduction of the effluent's organic matter when compared with the average COD of $1.35\,\text{kg/m}^3$ achieved in open-loop. The results show that it is possible to increase the biogas production of UASB reactors and improve their COD removal efficiency.

Analysing the reference inputs, we note that the influent flowrate reference Q^r_{in} saturates to its upper bound, while the wastage flowrate reference Q^r_{w} stays between the limits (although still higher than its nominal value). The input saturation is not surprising, given the linear objective of maximizing methane production from Section 3. We conjecture that the biogas production can be further increased if the flowrate limits can be relaxed (e.g., by having a larger collection tank).

4.2 Closed-loop operation of the UASB reactor (nominal scenario)

The main simulation results for the closed-loop operation of the UASB are shown in Figure 7. For the period shown, the average biogas production in open loop is $15.18\,\text{m}^3\text{/d}$, while the closed-loop operation leads to an increased production closer to the $24.43\,\text{m}^3\text{/d}$ reference. Specifically, the PID and MPC controllers produce $24.87\,\text{m}^3\text{/d}$ and $24.30\,\text{m}^3\text{/d}$ of biogas, respectively, on average. Thus, the closed-loop operation leads to over 60% increase in the biogas production when compared to the open-loop operation. Regarding effluent quality, we note that both controllers are capable of maintaining COD_{eff} concentrations close to the optimal reference, and below the desired limit: both achieve $0.77\,\text{kg/m}^3$

of COD, on average, representing a 43% reduction over the 1.35 kg/m^3 of COD achieved by the open-loop operation. Given the average COD_{in} of 8.65 kg/m^3, the open-loop system demonstrates an 84.4% organic matter removal efficiency, while the controlled system has a 91% efficiency. These result indicate that both controllers are capable of reacting to the influent disturbances and maintain the UASB reactor around the desired operating point.

The control actions determined by the controllers are also shown in Figure 7 (left). In closed-loop operation, both Q_{in} and Q_{w} are increased beyond their open-loop nominal values. Specifically, the influent flowrate Q_{in} is kept close to the 7 m^3/d reference during the whole simulation, with a drop observed at the end for the MPC configuration: the average influent flowrates ($Q_{\text{in,avg}}$) are 6.92 m^3/d, for the PID, and 6.80 m^3/d, for the MPC. Conversely, the waste flowrate Q_{w} deployed by the MPC is shown to oscillate around the 1.12 m^3/d reference, whereas the PID deploys an almost constant value for this control handle: the average waste flowrates ($Q_{\text{w,avg}}$) are 1.28 m^3/d, for the PID, and 1.23 m^3/d, for the MPC. Therefore, although both controllers have similar performances, the MPC is slightly more economical.

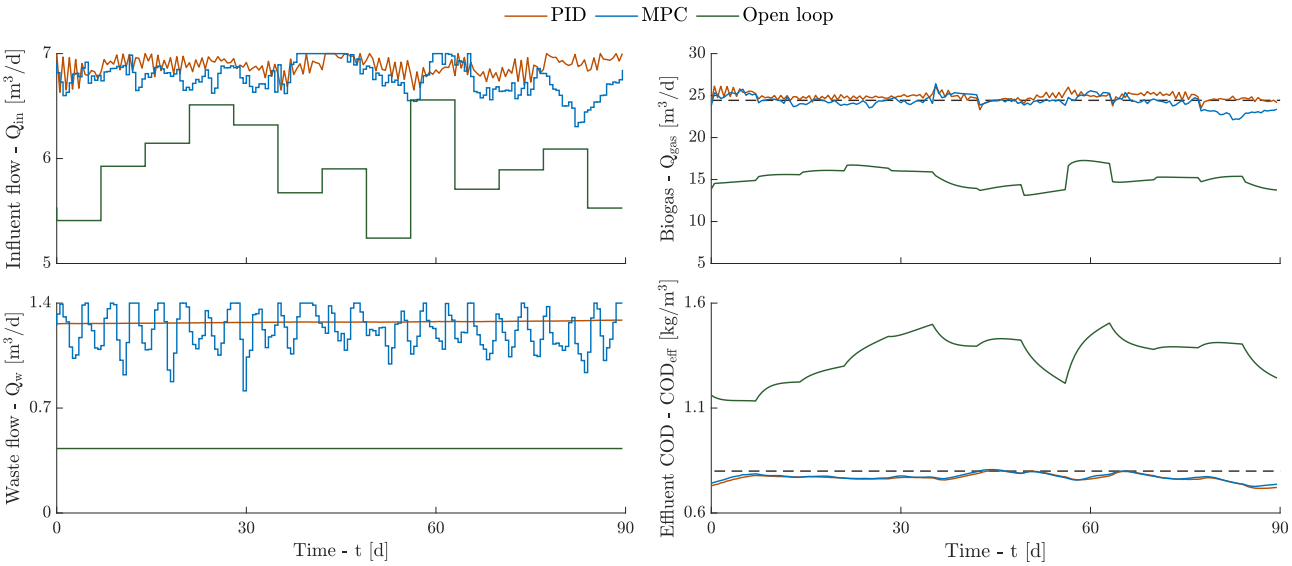


Figure 7: Nominal scenario: inputs (left) and a selection of outputs (right) of the UASB reactor under open-loop operation and closed-loop operation. The dashed lines indicate the optimal reference values from the OPO.

In both configurations, the controlled system results in a more stable biogas production when compared to the open loop system, despite being subject to noisy measurements and the same influent disturbances. Because the biogas production is mostly from Zone B, and the volume V^{A} of Zone A increases with the solids entering the UASB, the control strategies implemented by these controllers are indirectly focused on removing sludge. Using this control strategy, the volume V^{B} of Zone B is balanced and directly leads to more biogas being produced. A higher biogas production indicates that more organic matter is being consumed, thus explaining the improved COD. Finally, the methane production achieved by the closed-loop systems are shown in Figure 8. The results indicate that both controllers are capable of increasing the methane production: for the period shown, the PID and MPC achieve an average methane production (MP_{avg}) of 5.85 kg/d and 5.77 kg/d, respectively. This represent increases of 12.07% and 10.54%, respectively, over the 5.22 kg/d average production achieved by the open-loop configuration. Table 2 summarises the simulation results.

Table 2: Nominal scenario: performance metrics. Percentages are relative to the open-loop values.

	$Q_{\text{gas,avg}}$ (m^3/d)	$\text{COD}_{\text{eff,avg}}$ (kg/m^3)	$Q_{\text{in,avg}}$ (m^3/d)	$Q_{\text{w,avg}}$ (m^3/d)	MP_{avg} (kg/d)
Open loop	15.18	1.35	5.92	0.43	5.22
PID control	24.87 (+63%)	0.77 (-43%)	6.88 (+16%)	1.27 (+195%)	5.85 (+12%)
MPC control	24.30 (+60%)	0.77 (-43%)	6.77 (+14%)	1.22 (+184%)	5.77 (+10%)

Moving-horizon estimator: The output-feedback MPC in this work is based on state estimates produced by a MHE; thus, we briefly discuss its performance in the following. The results (Figure 9) show that the estimator is able to accurately reconstruct the true value of the outputs, effectively filtering out the measurement noise. An exception occurs with biogas Q_{gas}: for this output signal, the MHE overfits the measurement data, thus producing slightly less accurate estimates.

Learning and Nonlinear Models - Journal of the Brazilian Society on Artificial Intelligence (SBIA), Vol. 24, Iss. 1, pp. 46–59, 2026
https://doi.org/10.21528/lnlm-vol24-no1-art4 © Brazilian Society on Artificial Intelligence

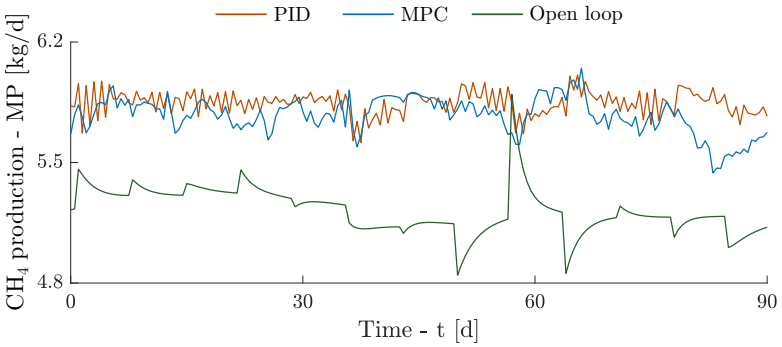


Figure 8: Nominal scenario: methane production (MP) from the UASB reactor under open-loop and close-loop operation.

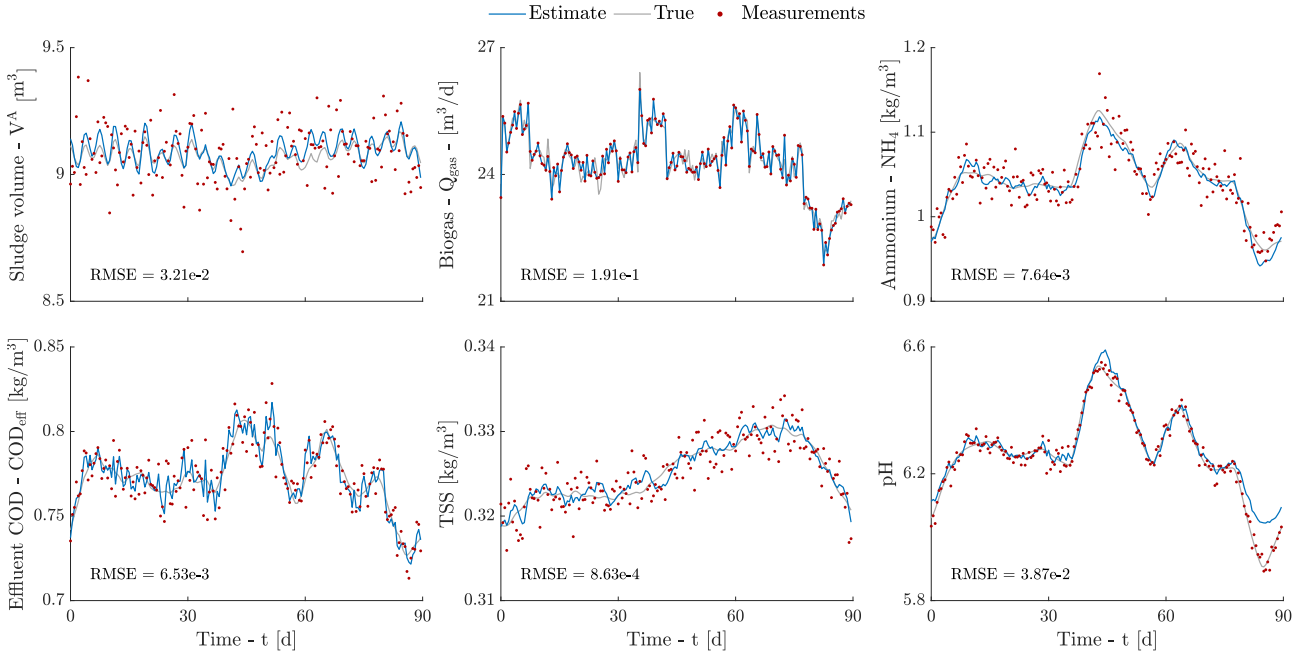


Figure 9: Nominal scenario: output estimates, their true values, and the (noisy) measurements filtered by the MHE.

4.3 Closed-loop operation of the UASB reactor (extreme scenario)

In the following, we present the results of operating the UASB reactor when subjected to extreme influent conditions. The main results are shown in Figure 10, with extreme events reflected by the sudden drops of effluent biogas and COD. Under open-loop operation, the effluent biogas flowrate is 14.71 m^3/d, on average, reaching a minimum of 6.18 m^3/d during the extreme events. The open-loop average COD_{eff} improves over the nominal scenario, however reaching peaks of up to 1.54 kg/m^3 in this case. Under closed-loop operation, the PID controller is able to maintain the biogas production at an average of 23.33 m^3/d, keeping Q_{gas} at the reference or slightly above it for most of the simulation. The average COD_{eff} achieved by the PID is 0.88 kg/m^3; higher than the OPO reference, although still 27.3% lower than the open-loop configuration. The MPC controller produces 22.85 m^3/d of biogas and keeps the COD_{eff} under the setpoint for most of the evaluation period, with a 0.80 kg/m^3 on average. The Q_{in} from the PID controller is kept at the upper bound for almost the entire simulation, while the MPC tends to saturate the inputs only during the extreme events.

The simulation results are summarised in Table 3, where we also show the average methane production under the different operations. While the extreme events clearly degrade open-loop performance, the results show that the closed-loop performance is only slightly affected; thus demonstrating the capacity of feedback controllers to react to external disturbances. Again, we conclude that both controllers are capable of reacting to the influent disturbances and maintain the UASB reactor around the desired operating point, with the MPC being more economical.

5 Conclusions

This work presented a control strategy for maximising the methane production of a UASB reactor treating blackwater. We developed a dynamic model based on the ADM1, which is then calibrated to better represent the dynamics of a real

Learning and Nonlinear Models - Journal of the Brazilian Society on Artificial Intelligence (SBIA), Vol. 24, Iss. 1, pp. 46–59, 2026
https://doi.org/10.21528/lnlm-vol24-no1-art4 © Brazilian Society on Artificial Intelligence

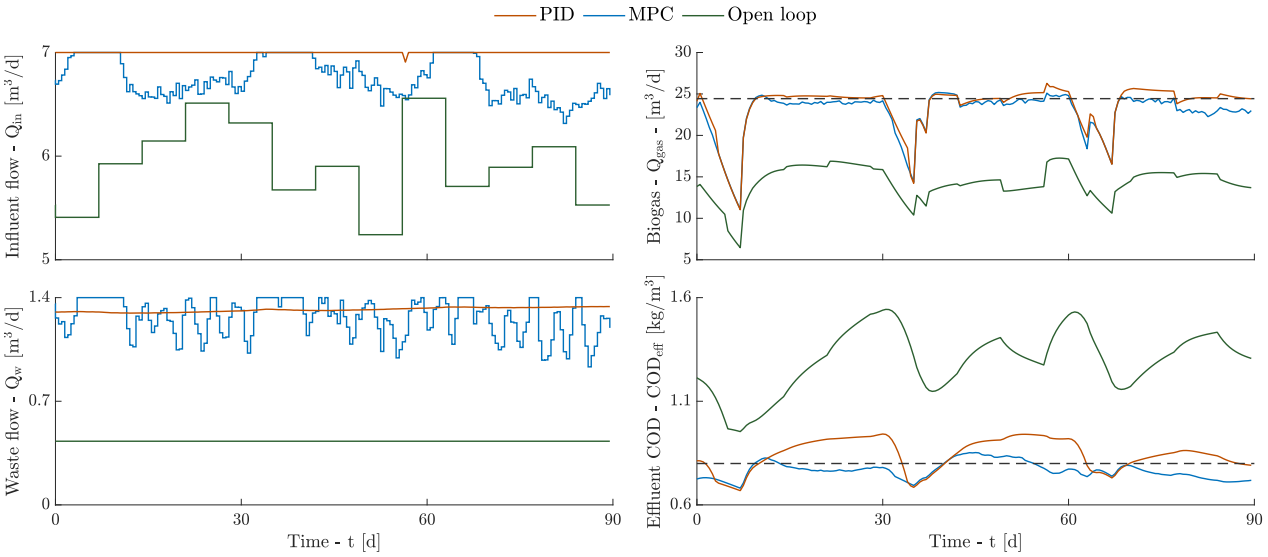


Figure 10: Extreme scenario: inputs (left) and a selection of outputs (right) of the UASB reactor under open-loop operation and closed-loop operation. The dashed lines indicate the optimal reference values from the OPO.

Table 3: Extreme scenario: performance metrics. Percentages are relative to the open-loop values.

	$Q_{gas,avg}$ (m^3/d)	$COD_{eff,avg}$ (kg/m^3)	$Q_{in,avg}$ (m^3/d)	$Q_{w,avg}$ (m^3/d)	MP_{avg} (kg/d)
Open loop	14.71	1.21	5.92	0.43	4.90
PID control	23.33 (+58%)	0.88 (-27%)	7.00 (+18%)	1.32 (+207%)	5.41 (+10%)
MPC control	22.85 (+55%)	0.80 (-33%)	6.75 (+14%)	1.26 (+193%)	5.36 (+09%)

treatment plant located in Helsingborg, Sweden. We investigated a control solution in which we first obtain optimal setpoints that correspond to increased methane production, and then employ feedback control to regulate the system to these setpoints. For the task, we consider two feedback control strategies: a PID and an output-feedback MPC. Finally, we showcased the controllers in different simulation experiments.

The results show that the UASB reactor admits an operation that results in increased biogas production and organic matter reduction when compared to its nominal open-loop operation. Specifically, our first simulation results show that the controlled plant achieves more than 60% increase in the biogas production while achieving 43% reduction of effluent COD when compared to the open-loop operation. The control solution is also capable of producing up to 12% more methane, while reaching almost 91% of organic matter removal efficiency in both strategies. This demonstrates the potential of the UASB reactor to produce methane efficiently, while maintaining effluent quality, by adjusting its influent and waste flows in real-time. Both control approaches have similar setpoint tracking performances, with the MPC being slightly more economical and robust to influent disturbances. The MPC strategy tends to use less pumping than the PID solution, while also being able to achieve a more desirable effluent quality during the extreme event scenario. The MPC performance relies on the state estimations of the MHE module. Therefore the better the estimates, the better efficiency results. Apart from that, the MHE estimates can give insights of the internal behaviour of the reactor given the measurements.

In this sense, the controlled version of the reactor guarantees a consistent production of biogas and methane, together with the effluent quality, allowing for the recovery of energy and other resources. The dynamical model, together with the estimation and control platforms, represent an initial step towards integrated digital solutions for the monitoring and automation of WRRFs, such as Digital Twins [4]. As future work, we plan to validate our results in different UASB reactors and investigate alternative control strategies capable of simultaneously optimising the concentration of nutrients on both the wastage and the effluent flows, thus allowing for further resource recovery.

Acknowledgment

This research has been finacially supported by the Fundação Cearense de Apoio ao Desenvolvimento Científico e Tecnológico (FUNCAP). We thank Saleh Abuzir and Filipe P. Farias for their contributions during the work.

References

[1] International Energy Agency. "Global Energy Review 2026", 2026. Licence: CC BY 4.0. [Online]. Available: https://www.iea.org/reports/global-energy-review-2026. Accessed: 2026-05-19.

[2] B. J. Van Ruijven, E. De Cian and I. Sue Wing. "Amplification of future energy demand growth due to climate change". *Nature communications*, vol. 10, no. 1, pp. 2762, 2019.

[3] International Energy Agency. "Electricity 2026", 2026. Licence: CC BY 4.0. [Online]. Available: https://www.iea.org/reports/electricity-2026. Accessed: 2026-05-19.

[4] M. Garrido-Baserba, D. L. Sedlak, M. Molinos-Senante and et al. "Using water and wastewater decentralization to enhance the resilience and sustainability of cities". *Nature Water*, vol. 2, no. 10, pp. 953–974, 2024.

[5] M. Molinos-Senante, S. Cantera and R. Lebrero. "A comparative techno-economic analysis review of gas valorization in the transition from wastewater treatment plants to water resource recovery facilities". *Current Opinion in Environmental Sustainability*, vol. 83, pp. 101691, 2026.

[6] X. F. Almansa, R. Starostka, L. Raskin, G. Zeeman, F. De Los Reyes III, J. Waechter, D. Yeh and T. Radu. "Anaerobic digestion as a core technology in addressing the global sanitation crisis: challenges and opportunities". *Environmental Science & Technology*, vol. 57, no. 48, pp. 19078–19087, 2023.

[7] I. Bisschops, H. Kjerstadius, B. Meulman and M. Van Eekert. "Integrated nutrient recovery from source-separated domestic wastewaters for application as fertilisers". *Current Opinion in Environmental Sustainability*, vol. 40, pp. 7–13, 2019.

[8] L. André, A. Pauss and T. Ribeiro. "Solid anaerobic digestion: State-of-art, scientific and technological hurdles". *Bioresource Technology*, vol. 247, pp. 1027–1037, 2018.

[9] G. Silvestre, B. Fernández and A. Bonmatí. "Significance of anaerobic digestion as a source of clean energy in wastewater treatment plants". *Energy Conversion and Management*, vol. 101, pp. 255–262, 2015.

[10] R. Jayabal and R. Sivanraju. "Wastewater treatment for energy conservation and zero carbon footprint: A review". *Energy Science & Engineering*, vol. 13, no. 7, pp. 3806–3820, 2025.

[11] T. Bressani-Ribeiro and C. A. L. Chernicharo. "Upflow anaerobic sludge blanket reactors". In *Anaerobic Treatment of Domestic Wastewater: Present Status and Potentialities*, edited by M. C. Tomei and J. M. Garrido. IWA Publishing, 2024.

[12] S. Abuzir, L. Gren, M. Domini, G. Bertanza, Å. Davidsson and H. Kjerstadius. "Performance of a full-scale anaerobic UASB digester treating blackwater from an urban city district in Helsingborg, Sweden". *Cleaner Water*, vol. 4, pp. 100082, 2025.

[13] A. G. Sheik, E. Tejaswini and S. R. Ambati. "Design of intelligent control strategies for full-scale wastewater treatment plants with struvite unit". *Journal of Water Process Engineering*, vol. 49, pp. 103104, 2022.

[14] M. Ruano, J. Ribes, A. Ruiz-Martinez, A. Seco and A. Robles. "An advanced control system for nitrogen removal and energy consumption optimization in full-scale wastewater treatment plants". *Journal of Water Process Engineering*, vol. 57, pp. 104705, 2024.

[15] T. Ujazdowski, R. Piotrowski and M. Banach. "A stochastic approach for the solution of single and multi–objective optimisation problems of biological processes in sequencing batch reactor". *Journal of Process Control*, vol. 140, pp. 103266, 2024.

[16] O. B. Neto, M. Mulas, I. Harjunkoski and F. Corona. "Predictive control of wastewater treatment plants as energy-autonomous water resource recovery facilities". *Control Engineering Practice*, vol. 172, pp. 106888, 2026.

[17] T. Hägglund and J. L. Guzmán. "Give us PID controllers and we can control the world". *IFAC-PapersOnLine*, vol. 58, no. 7, pp. 103–108, 2024.

[18] K. J. Astrom and R. M. Murray. *Feedback Systems: An Introduction for Scientists and Engineers*. Princeton University Press, USA, 2020.

[19] L. Åmand, G. Olsson and B. Carlsson. "Aeration control – a review". *Water Science and Technology*, vol. 67, no. 11, pp. 2374–2398, 06 2013.

[20] S. Revollar, R. Vilanova, M. Francisco and P. Vega. "PI Dissolved Oxygen control in wastewater treatment plants for plantwide nitrogen removal efficiency". *IFAC-PapersOnLine*, vol. 51, no. 4, pp. 450–455, 2018.

[21] S. Du, Q. Yan and J. Qiao. "Event-triggered PID control for wastewater treatment plants". *Journal of Water Process Engineering*, vol. 38, pp. 101659, 2020.

[22] Z. He, S. Li, D. Hu and Y. Man. "Low-carbon, green, and economic scheme for wastewater treatment process based on multi-objective optimal control". *Chemical Engineering Science*, vol. 306, pp. 121297, 2025.

[23] J. B. Rawlings, D. Q. Mayne and M. M. Diehl. *Model Predictive Control: Theory, Computation, and Design*. Nob Hill Publishing, Madison, WI, second edition, 2017.

[24] D. Q. Mayne. "Model predictive control: Recent developments and future promise". *Automatica*, vol. 50, no. 12, pp. 2967–2986, 2014.

[25] I. Kalogeropoulos, A. Alexandridis and H. Sarimveis. "Economic oriented dynamic matrix control of wastewater treatment plants". *Journal of Process Control*, vol. 118, pp. 202–217, 2022.

[26] S. Du, Q. Zhang, H. Han, H. Sun and J. Qiao. "Event-triggered model predictive control of wastewater treatment plants". *Journal of Water Process Engineering*, vol. 47, pp. 102765, 2022.

[27] Y. Yang, X. Wang, Y. Wu, F. Li, Z. Maletskyi, S. Chen, M. Tang and Z. Song. "Integration of soft sensors and model predictive control for denitrification at a full-scale wastewater treatment plant". *Journal of Water Process Engineering*, vol. 72, pp. 107422, 2025.

[28] H. Liu, X. Li, Y. Chen, J. Zhang, J. Li, J. Hui, J. Liu and W. An. "Adaptive real-time dosing strategy for advanced phosphorus removal using model predictive control and time-series analysis in WWTPs". *Water Research*, p. 125925, 2026.

[29] H.-G. Han, C.-Y. Wang, H.-Y. Sun and J.-F. Qiao. "Data-based robust model predictive control for wastewater treatment process". *Journal of Process Control*, vol. 118, pp. 115–125, 2022.

[30] U. K. Ramesh, P. R. Brahmbhatt, S. Avraamidou and H. S. Ganesh. "Neural network and integer programming-based Model Predictive Control for a wastewater treatment process". *Journal of Process Control*, vol. 162, pp. 103717, 2026.

[31] Y. Wang, H.-Y. Sun and H.-G. Han. "Data-driven soft constrained model predictive control with disturbance rejection for wastewater treatment processes". *Journal of Process Control*, vol. 160, pp. 103656, 2026.

[32] H.-G. Han, C. Chen, H.-Y. Sun and J.-F. Qiao. "Multi-objective integrated optimal control for a wastewater treatment process". *Control Engineering Practice*, vol. 128, pp. 105296, 2022.

[33] H. Zhou, S. Liu, J. Ren, J. Zhang and H. Li. "Multivariable event-triggered predictive control based on recursive bilinear subspace identification for wastewater treatment processes". *Desalination and Water Treatment*, vol. 295, pp. 105–124, 2023.

[34] S. Mu, Y. Zeng and P. Wu. "Multivariable control of anaerobic reactor by using external recirculation and bypass ratio". *Journal of Chemical Technology & Biotechnology*, vol. 83, no. 6, pp. 892–903, 2008.

[35] S. Amornraksa, C. Panjapornpon, S. K. Maity, M. Sriariyanun and A. Tawai. "AOPC-based control for efficient uncertainty mitigation in UASB wastewater treatment with multiple manipulated variables and distributed biomass integration". *Computers & Chemical Engineering*, vol. 187, pp. 108735, 2024.

[36] D. J. Batstone, J. Keller, I. Angelidaki, S. V. Kalyuzhnyi, S. G. Pavlostathis, A. Rozzi, W. Sanders, H. Siegrist and V. A. Vavilin. "The IWA Anaerobic Digestion Model No.1 (ADM1)". *Water Science and technology*, vol. 45, no. 10, pp. 65–73, 2002.

[37] C. A. de Lemos Chernicharo. *Anaerobic reactors*. IWA publishing, 2007.

[38] R. Boiocchi, Q. Zhang, M. Gao and Y. Liu. "Modeling and optimization of an upflow anaerobic sludge blanket (UASB) system treating blackwaters". *Journal of Environmental Chemical Engineering*, vol. 10, no. 3, pp. 107614, 2022.

[39] J. Nocedal and S. J. Wright. *Numerical Optimization*. Springer Series in Operations Research and Financial Engineering. Springer, New York, NY, second edition, 2006.

[40] L. F. Shampine and M. W. Reichelt. "The MATLAB ODE Suite". *SIAM Journal on Scientific Computing*, vol. 18, no. 1, pp. 1–22, 1997.

[41] K. V. Gernaey, U. Jeppsson, P. A. Vanrolleghem and J. B. Copp. *Benchmarking of control strategies for wastewater treatment plants*. IWA publishing, 2014.

[42] K. J. Aström and T. Hägglund. *Advanced PID control*. John Wiley & Sons, 2005.

[43] J.-J. E. Slotine, W. Li *et al.*. *Applied nonlinear control*, volume 199. Prentice hall Englewood Cliffs, NJ, 1991.